

# Accelerating Targeted Hard-Label Adversarial Attacks in Low-Query Black-Box Settings

Arjhun Swaminathan<sup>1,2</sup>   Mete Akgün<sup>1,2</sup>  
 {arjhun.swaminathan, mete.akguen}@uni-tuebingen.de

<sup>1</sup>Medical Data Privacy and Privacy-preserving Machine Learning (MDPPML), University of Tübingen

<sup>2</sup>Institute for Bioinformatics and Medical Informatics (IBMI), University of Tübingen

## Abstract

Deep neural networks for image classification remain vulnerable to adversarial examples – small, imperceptible perturbations that induce misclassifications. In black-box settings, where only the final prediction is accessible, crafting targeted attacks that aim to misclassify into a specific target class is particularly challenging due to narrow decision regions. Current state-of-the-art methods often exploit the geometric properties of the decision boundary separating a source image and a target image rather than incorporating information from the images themselves. In contrast, we propose Targeted Edge-informed Attack (TEA), a novel attack that utilizes edge information from the target image to carefully perturb it, thereby producing an adversarial image that is closer to the source image while still achieving the desired target classification. Our approach consistently outperforms current state-of-the-art methods across different models in low query settings (nearly 70% fewer queries are used), a scenario especially relevant in real-world applications with limited queries and black-box access. Furthermore, by efficiently generating a suitable adversarial example, TEA provides an improved target initialization for established geometry-based attacks.

## 1 Introduction

Deep neural networks have achieved remarkable performance in image classification tasks, powering applications from autonomous systems [2, 5] to medical diagnostics [9, 12]. However, they have repeatedly been shown to be vulnerable to adversarial examples [11, 23]. These are small, often imperceptible perturbations to a correctly classified image that cause a misclassification. Although many of these attacks assume white-box access to a model’s internals, hard-label (decision-based) attacks offer a more challenging yet practical setting where only the top-1 predicted label is observed. This limited-feedback scenario commonly arises in commercial APIs [13]. In this realm, targeted attacks, which push the model’s prediction to a specific target class, are inherently more difficult since the decision regions corresponding to the specific target classes are usually narrower and more isolated.

In black-box settings, targeted hard-label attacks have become an active area of research, with several techniques proposed in the literature, with state-of-the-art methods relying on the geometry of the decision boundary separating the source image from the target class. Geometry-informed attacks traverse in a lower-dimensional space and fall into two categories: *Boundary Tracing Attacks* and *Gradient Estimation Attacks*. Boundary Tracing Attacks ([3, 4, 18, 22]) perform walks along the decision boundary while Gradient Estimation Attacks ([6, 14, 16, 17, 19, 24, 25]) perform the same walks but using information about the approximate tangent/normal to the decision boundary in a local neighborhood to their adversarial image. Although powerful for local refinement, both approaches tend to burn through queries when the source image lies far from a given adversarial image in a

target class, wasting many queries before reaching a narrow region where local geometry can more effectively be leveraged.

Further, in practice, many real-world scenarios such as commercial pay-per-query APIs, impose severe constraints on the number of queries that can be made to a target model in a specified time. Often practical query limits may be on the order of a few hundred to fewer than a few thousand queries. Under these conditions, the limited feedback available makes it difficult to effectively use information about the local decision boundary geometry in the early stages of an attack. When the decision space is still wide, movement along restricted lower dimensional spaces leads to limited incremental progress, and gradient estimation methods often use queries in estimating local gradients by sampling predictions in a local neighborhood instead of moving. This raises a pressing need to develop methods that are efficient in the low-query regime. In a high query setting, this would also lead us to a good starting point to employ the geometry-informed methods since we arrive at a good adversarial point quickly and can use the geometry-informed information more effectively. To this end, we propose Targeted Edge-Informed Attack (TEA), a novel targeted adversarial attack designed for hard-label black-box scenarios within a restricted query budget. Rather than depending on the local properties of the decision boundary, TEA leverages the intrinsic features of the target image itself - specifically, the edge information obtained using Sobel filters [21] help identify prominent structural features in the target image. Edges encode high-magnitude spatial gradients that delineate object boundaries [21]. Research has shown that early layers fire on oriented edge filters [1, 26], and that shape/edge cues remain predictive even when textures are suppressed [10]. The core idea is to preserve these low-level features, while applying perturbations to the non-edge regions of an image, allowing us to stay in the target class while pushing the adversarial image towards the source image. When our progress plateaus, evidenced by a series of consecutive queries that fail to achieve further reduction in distance while maintaining target class prediction, one can switch to current state-of-the-art geometry-informed methods for a local refinement procedure. Hence we make the following contributions:

**Global initialization for low-query efficiency:** We introduce an edge-informed perturbation strategy, enabling rapid progress toward the source image in the early stages of an adversarial attack. This strategy involves a two-step process: First, a global edge-informed search is performed, and then, edge-informed updates are applied to small patches using Gaussian weights.

**Empirical validation under strict query budgets:** We perform extensive evaluations on the ImageNet validation dataset [7] across four architectures (ResNet-50 [12], ResNet-101 [12], VGG16 [20], and ViT [8]). Our attack consistently outperforms existing state-of-the-art hard-label methods, including HSJA, Adaptive History-driven Attack (AHA) [15], CGBA, and CGBA-H, under realistic query budgets (fewer than 1000 queries). To achieve a 60% reduction in distance from a target image to a source image, TEA required on average 251 queries across the four models - 70% fewer than AHA (the second fastest), which required 845 queries.

The rest of this paper is structured as follows. Section 2 reviews related targeted hard-label adversarial attacks. Section 3 describes our methodology, while Section 4 presents experimental results. Finally, Section 5 discusses potential limitations and outlines directions for future research.

## 2 Related Works

Early work in the realm of targeted hard-label adversarial attacks consisted of seminal work: Boundary Attack (BA) [3], which proposed a method of traversing the decision boundary that separates an adversarial image from a source image. Building on this framework, BiasedBA [4] incorporated directional priors, such as perceptual and low-frequency biases, to restrict the search to more promising regions. BA with Output Diversification Strategy (BAODS) [24] integrates diverse gradient-like signals into the exploration process of BA, thereby strengthening the original method.

Following these foundational methods, Hybrid Attack (HA) [22] employed a combination of heuristic search strategies to balance global exploration and local refinement. Advancing toward more gradient-centric techniques, qFool [16] leverages the local flatness of decision boundaries to streamline the attack process. Meanwhile, HopSkipJumpAttack (HSJA) [6] locally approximates the normal to the decision boundary to “jump off” from it before progressing toward the source image. Complementarily, Tangent Attack exploits locally estimated tangents of the decision surface to steer the adversarial perturbation toward the source image. Addressing the challenges posed by high-

dimensional input spaces, Query Efficient Boundary Attack (QEBA) [14] projects gradient estimation into lower-dimensional subspaces, such as the frequency domain, thus significantly reducing the number of required queries.

Incorporating historical query information, Adaptive History-driven Attack (AHA) [15] adapts its search trajectory based on previous successes and failures, while Decision-based query Efficient Adversarial Attack based on boundary Learning (DEAL) [6] employs an evolutionary strategy that concentrates queries on promising regions of the input space. SurFree [18] demonstrated that using 2D planes and semicircular trajectories toward the source image was an effective strategy. This was based on the fact that under the assumption of a flat decision boundary, the point on the boundary that is closest to the source image is precisely where the semicircular trajectory intersects it. Building on this idea, Curvature-Aware Geometric black-box Attack (CGBA) and its variant that is more suited for targeted attacks - CGBA-H [19], use normal estimation at the decision boundary to select the traversal plane. To the best of our knowledge, CGBA, and CGBA-H serve as the current state of the art in decision-based adversarial attacks.

### 3 Methodology

In this section, we formalize the hard-label attack setting and detail our attack, which drastically reduces early query cost, especially when the target image is far from the source image, and exists in a wider decision space. Once the adversarial image achieves a good distance and reaches a narrow decision space, one can use the image as an initialization and continue refining with existing geometric-based methods.

**Problem Statement.** We consider a hard-label image classifier

$$f : [0, 1]^{C \times H \times W} \rightarrow \mathbb{R}^K, \quad (1)$$

where  $C$  denotes the number of color channels,  $H$  and  $W$  are the image height and width, and the classifier distinguishes among  $K$  classes. For any query image  $x$ , we do not observe its continuous output (e.g., logits or probabilities) but only the predicted label index

$$\hat{y}(x) = \arg \max_{1 \leq k \leq K} [f(x)]_k. \quad (2)$$

Let  $x_s$  be a *source* image correctly classified as  $y_s$ . In a *targeted* attack, we start with a *target* image  $x_t$  (correctly classified as  $y_t$ ). Our goal is to find an adversarial image  $x_{\text{adv}}$  that is as close as possible to  $x_s$  (in the  $\ell_2$  norm) while maintaining the target classification, i.e.,

$$x_{\text{adv}} = \arg \min_x \|x - x_s\|_2, \quad \text{subject to} \quad \hat{y}(x) = y_t. \quad (3)$$

We propose a two-part procedure for perturbing the target image  $x_t$  to get closer to  $x_s$  while maintaining adversarial requirements. First, a *global* edge-informed search coarsely aligns major image regions. Second, a *patch-based* edge-informed search further perturbs local regions in our adversarial image. Note that neither step leverages local decision boundary geometry or gradient estimation, which are typically beneficial only when the adversarial image lies near a narrow decision space and when movements towards the source image are unlikely to maintain classification. This approach avoids burning queries in a wider decision space.

#### 3.1 Global Edge-Informed Search

The global perturbation step aims to coarsely align  $x_t$  towards  $x_s$  by modifying predominantly smooth, non-edge areas, thereby preserving crucial edge structures that help maintain target classification.

**Soft Edge Mask.** To this end, we detect edges in  $x_t$  using the Sobel operator [21], as depicted in Figure 1. A subsequent blurring operation yields a *soft edge mask*  $M_{\text{edge}}$ , where  $M_{\text{edge}}(i, j) \in [0, 1]$  has values close to 1 at edge locations and gradually transitions to 0 in smoother regions. We describe this in Algorithm 1.

**Global Interpolation.** Starting from  $x_0 = x_t$ , we perform iterative updates:

$$x_{k+1} \leftarrow x_k + \alpha(x_s - x_k) \odot (I - M_{\text{edge}}), \quad (4)$$

---

**Algorithm 1** Soft Edge Mask

---

```

1: Inputs: Image  $x$ , edge thresholds  $\{T_\ell, T_h\}$ , Gaussian blur kernel size  $b$ , intensity factor  $\gamma$ , small constant  $\epsilon$ 
2: Output: Soft edge mask  $M_{\text{edge}}$ 
3:  $x^{\text{gray}} \leftarrow \text{GrayScale}(x)$ 
4:  $(s_x, s_y) \leftarrow (\text{Sobel}(x^{\text{gray}}, 0), \text{Sobel}(x^{\text{gray}}, 1))$ 
5:  $G \leftarrow (s_x^2 + s_y^2)^{1/2}$ 
6:  $G \leftarrow 255 \cdot (G / (\max_{i,j}(G) + \epsilon))$ 
7:  $\text{edge\_mask}(i, j) \leftarrow \begin{cases} 255, & \text{if } T_\ell \leq G(i, j) \leq T_h, \\ 0, & \text{otherwise} \end{cases}$ 
8:  $\text{blurred} \leftarrow \text{GaussianBlur}(\text{edge\_mask}, (b, b))$ 
9:  $\text{norm} \leftarrow \text{Normalize}(\text{blurred})$ 
10:  $M_{\text{edge}} \leftarrow \gamma \cdot \text{norm}$ 
11: return  $M_{\text{edge}}$ 

```

---

where  $\odot$  denotes the element-wise (Hadamard) product. The scaling factor  $\alpha$  is optimized via a momentum based search. Masking out the edge regions in this update ensures that the interpolation primarily affects smooth areas, thus preserving the overall structure necessary for target classification. The complete procedure is summarized in Algorithm 2. Once the improvements stagnate, we transition to a local, patch-based refinement.

---

**Algorithm 2** Global Edge-Informed Search

---

```

1: Inputs: Source image  $x_s$ , target image  $x_t$ , soft edge mask  $M_{\text{edge}}$ , tolerance  $\tau$ , maximum queries  $qc_{\text{max}}$ , initial step factor  $\eta$ , momentum  $\mu$ 
2: Output: Adversarial image  $x_{\text{adv}}$  such that  $\hat{y}(x_{\text{adv}}) = y_t$ 
3:  $x_{\text{current}} \leftarrow x_t$ ,  $v \leftarrow 0$ , and  $d \leftarrow x_s - x_t$ 
4: Set step size:  $s \leftarrow \|d\|_2 \cdot \eta$ , and initialize query count  $qc \leftarrow 0$ 
5: while  $qc < qc_{\text{max}}$  and  $\|s\| \geq \tau$ 
6:    $v \leftarrow \mu \cdot v + (1 - \mu) \cdot d$ 
7:    $x_{\text{next}} \leftarrow x_{\text{current}} + s \cdot (v \odot (I - M_{\text{edge}}))$ 
8:    $qc \leftarrow qc + 1$ 
9:   if  $\hat{y}(x_{\text{next}}) = y_t$ 
10:     $x_{\text{current}} \leftarrow x_{\text{next}}$ 
11:     $s \leftarrow 1.1 \cdot s$ 
12:   else
13:     break
14: return  $x_{\text{current}}$ 

```

---

### 3.2 Patch-Based Edge-Informed Search

After the global interpolation, some subregions of the image may still display significant discrepancies from  $x_s$ . In the patch-based refinement, we partition the image into patches

$$\mathcal{P} \subseteq \{1, \dots, H\} \times \{1, \dots, W\}, \quad (5)$$

and for each patch, construct a local soft edge mask  $M_{\mathcal{P}}$  analogously to  $M_{\text{edge}}$ , but restricted to  $\mathcal{P}$ . Then, we apply a local interpolation:

$$\tilde{x}(\beta) = x_k + \beta(x_s - x_k) \odot G \odot (I - M_{\mathcal{P}}), \quad (6)$$

and search for the largest  $\beta$  such that  $\hat{y}(\tilde{x}(\beta)) = y_t$ . Here,  $G$  is a Gaussian weight applied across the patch to avoid artificial edges being created by our patches. This localized update is performed over multiple patches of varying sizes to steadily decrease the distance to the source image. The patch-based refinement is repeated until a termination criterion is met (e.g., 25 consecutive iterations with no further improvement). The corresponding illustration is depicted in Figure 1 and the relevant pseudocode is provided in Algorithm 3.

Figure 2 offers a visual summary of TEA. The figure depicts the adversarial image throughout our method, and displays also a hotspot of individual pixel differences from the source image.

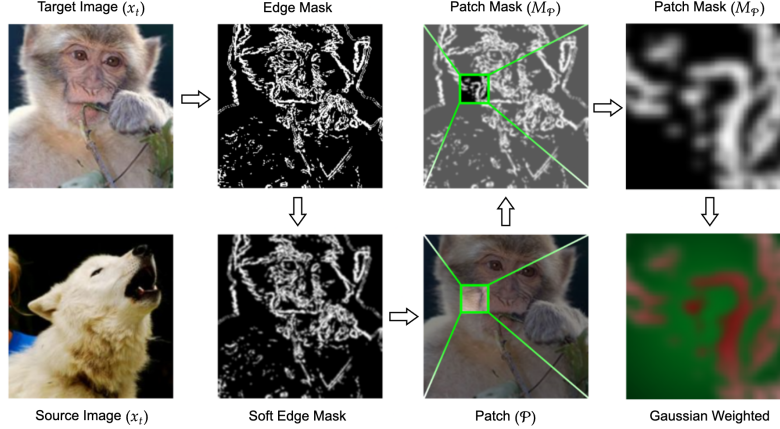


Figure 1: **Overview of Patch-Based Edge-Informed Search.** Edge information from the target image, obtained via the Sobel operator, is first blurred to generate a soft edge mask. A square patch is then selected and a Gaussian weighting function is applied. In the bottom right panel, the intensity of the modification is illustrated: dark red regions remain largely unchanged, while light green regions receive a more pronounced update. The lack of changes near the patch borders helps prevent the introduction of artificial edges.

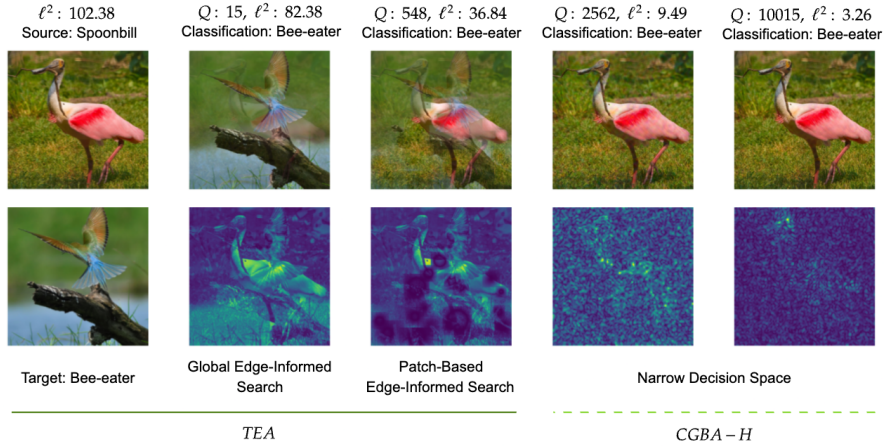


Figure 2: **Visualization of TEA on a source-target image pair.** The target image (initially classified as *Bee-eater*) is perturbed to resemble the source image (classified as *Spoonbill*), while preserving its original *Bee-eater* label. Global Edge-Informed Search efficiently applies edge-aware perturbations using only 15 queries to achieve a  $\approx 20\%$  reduction in distance to the source. Patch-Based Edge-Informed Search introduces localized, edge-aware modifications to small image regions, as seen in the hotspot of changes. Further refinement utilizing CGBA-H is illustrated in the narrow decision space.

## 4 Experiments

In this section, we present our empirical evaluation on the ImageNet ILSVRC2012 dataset, benchmarking *TEA* against existing targeted hard-label attack strategies. In what follows, we describe our experimental setup and metrics, then detail the performance of each method under a range of query budgets. Our findings indicate that *TEA* achieves efficient distance reduction to the source image, particularly in the early query regime, before switching to the current state-of-the-art geometry-based attack *CGBA-H* for further refinement in a narrow decision space.

---

**Algorithm 3** Patch-Based Edge-Informed Search

---

```
1: Inputs: Source image  $x_s$ , current adversarial image  $x_{adv}$ , soft edge mask  $M_{edge}$  (from  
   create_soft_edge_mask), minimum patch size  $p_{min}$ , maximum patch size  $p_{max}$ , step factor  $\eta$ , mo-  
   mentum  $\mu$ , maximum calls  $N_{max}$   
2: Output: Refined adversarial image  $x_{adv}$   
3:  $n_{break} \leftarrow 0$   
4: while  $n_{break} < 25$   
5:    $D \leftarrow \text{AvgPool}(|x_s - x_{adv}|)$   
6:   Select high-difference indices from  $D$  and choose a random center  $(i_c, j_c)$   
7:    $p \leftarrow \text{randInt}(p_{min}, p_{max})$ ;  $\mathcal{P} \leftarrow \{(i, j) \mid |i - i_c| \leq \lfloor p/2 \rfloor, |j - j_c| \leq \lfloor p/2 \rfloor\}$   
8:    $M_{\mathcal{P}}(i, j) \leftarrow \begin{cases} 1, & (i, j) \in \mathcal{P}, \\ 0, & \text{otherwise.} \end{cases}$   
9:    $x_{patch} \leftarrow \text{Patch}(x_{adv}, \mathcal{P})$   
10:   $m_{patch} \leftarrow 0$ ,  $d_{base} \leftarrow \|x_s - x_{adv}\|_2$   
11:  for iteration = 1 to  $N_{max}$   
12:     $d_{local} \leftarrow \text{Patch}(x_s, \mathcal{P}) - x_{patch}$   
13:     $m_{patch} \leftarrow \mu \cdot m_{patch} + (1 - \mu) \cdot d_{local}$   
14:     $s_{patch} \leftarrow \eta \cdot \|x_s - x_{adv}\|_2$   
15:     $G \leftarrow \text{GaussianWeight}((i_c, j_c), \sigma = p/3)$   
16:     $\Delta x \leftarrow s_{patch} \cdot m_{patch} \odot (G \odot (1 - (M_{edge} \odot M_{\mathcal{P}})))$   
17:     $x_{patch}^+ \leftarrow x_{patch} + \Delta x$   
18:     $x_{temp} \leftarrow x_{adv} - x_{adv} \odot M_{\mathcal{P}} + x_{patch}^+ \odot M_{\mathcal{P}}$   
19:     $d_{new} \leftarrow \|x_s - x_{temp}\|_2$   
20:    if  $d_{new} \geq 0.999 \cdot d_{base}$   
21:      break  
22:    if  $\hat{y}(x_{temp}) = y_t$   
23:       $x_{patch} \leftarrow x_{patch}^+$   
24:       $x_{adv} \leftarrow \text{Replace}(x_{adv}, \mathcal{P}, x_{patch})$   
25:       $d_{base} \leftarrow d_{new}$   
26:       $n_{break} \leftarrow 0$   
27:    else  
28:       $n_{break} \leftarrow n_{break} + 1$   
29:    break  
30: return  $x_{adv}$ 
```

---

#### 4.1 Setup and Metrics

**Computational Resources.** The experiments were executed on a High-performance computing (HPC) Cluster. Each node on the cluster consisted of four NVIDIA GeForce GTX 1080 Ti GPUs (one GPU was allocated per source-target pair for a given attack).

**Dataset and Image Pairs.** We sample 1000 source-target image pairs from the ImageNet ILSVRC2012 validation set, ensuring the two images in each pair come from distinct classes. All images are resized to  $3 \times 224 \times 224$ . Each pair  $(x_s, x_t)$  contains a source image  $x_s$ , correctly classified under its label, and a target image  $x_t$ , also correctly classified under a different label. The attack goal is to modify  $x_t$  to approach  $x_s$  under the  $\ell_2$  norm while keeping the prediction unchanged.

**Target Models.** We evaluate our approach on four well-known classifiers: ResNet50 and ResNet101 (CNNs of varying depth), VGG16 (a CNN composed of repeated convolutional blocks), and ViT (a vision transformer that processes images as sequences of patches). These models represent a diverse set of architectures.

**Compared Methods.** We compare our method to four targeted hard-label attacks: HSJA, AHA, CGBA, and CGBA-H. For each method, the  $\ell_2$  distance to the source image is recorded after each set of queries, and along with the classification label of the perturbed target image.

**Evaluation Metrics.** Performance is quantified using three metrics. First, we compute the  $\ell_2$  distance from  $x_s$  to the adversarial example generated for each of the 1000 image pairs as queries progress. Second, the attack success rate (ASR) is defined as the fraction of image pairs for which an  $\alpha\%$  reduction in  $\|x_s - x_t\|$  is achieved within a given number of queries. Third, we also measure the performance of each method when there is a set fixed low-query budget by measuring the ASRs

for all  $\alpha$  when each method has used up 500 queries. Finally, we integrate the  $\ell^2$  distance versus queries curve to obtain the area under the curve (AUC), which provides an aggregated measure of how rapidly the distance is reduced.

**Implementation Details.** Our implementation employs a two-stage process. In the first stage, we perform our proposed methodology TEA, where edge-aware distortions are applied to the target image while preserving its classification, allowing a rapid reduction in distance to the source image. In the second stage, once the perturbation has brought the image into a narrow decision space, the method switches to CGBA-H for further refinement. The last query performed with TEA is referred to as the *turning point* throughout the study. We switch to CGBA-H since it consistently performs better than other methods in a high query setting across different architectures.

## 4.2 Results

**Average  $\ell_2$ -Distance vs. Queries.** Table 1 presents a comparative analysis of the median  $\ell_2$  distances achieved in the low-query regime—specifically, within the range defined by the average turning point computed over one thousand image pairs. This analysis underscores the rapid decrease in perturbation norm facilitated by TEA during the early query stages. Figure 3 extends this evaluation by depicting the average percentage reduction in the  $\ell_2$  distance against the queries used.

Table 1: Median  $\ell_2$  distances computed until the turning point across different architectures. Lower  $\ell^2$  values denote faster adversarial example generation.

Query	ResNet50					Query	ResNet101				
	HSJA	CGBA	CGBA-H	AHA	TEA		HSJA	CGBA	CGBA-H	AHA	TEA
100	92.797	88.857	83.104	80.438	<b>73.154</b>	100	90.962	81.376	85.623	82.574	<b>71.750</b>
200	88.715	87.165	79.348	75.344	<b>59.673</b>	200	88.194	74.738	84.246	77.869	<b>58.904</b>
300	88.604	71.054	86.236	74.168	<b>53.010</b>	300	87.954	70.676	83.750	71.874	<b>51.768</b>
400	88.199	67.091	85.579	71.479	<b>48.825</b>	400	87.222	67.051	82.483	68.803	<b>48.243</b>
500	87.724	64.172	84.897	68.671	<b>46.777</b>	500	87.356	63.717	81.543	66.169	<b>46.229</b>
602	87.203	83.937	66.774	61.168	<b>45.600</b>	592	87.133	80.339	64.528	61.134	<b>45.139</b>

Query	VGG16					Query	ViT				
	HSJA	CGBA	CGBA-H	AHA	TEA		HSJA	CGBA	CGBA-H	AHA	TEA
100	93.966	92.154	85.805	84.770	<b>75.634</b>	100	80.454	76.885	73.074	65.501	<b>65.347</b>
200	89.884	90.899	81.599	78.445	<b>61.148</b>	200	79.981	74.702	69.511	58.863	<b>54.851</b>
300	89.665	73.174	90.516	74.359	<b>54.977</b>	300	79.606	53.951	74.139	63.655	<b>49.164</b>
400	88.943	68.538	89.880	70.559	<b>50.940</b>	400	79.599	49.857	72.839	61.300	<b>46.139</b>
500	88.919	65.569	89.563	67.745	<b>48.943</b>	500	78.761	46.572	71.291	58.598	<b>44.347</b>
588	88.389	88.362	66.578	62.126	<b>47.484</b>	554	79.626	69.954	57.710	44.494	<b>43.422</b>

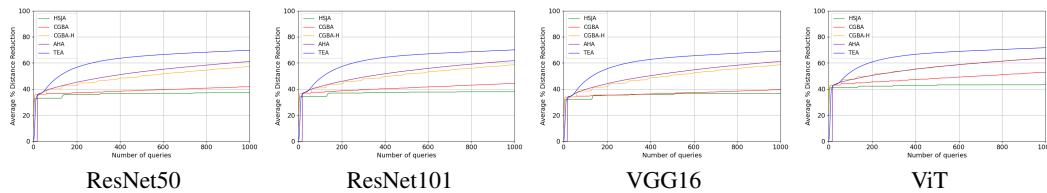


Figure 3: Average  $\ell_2$  distance reduction across different architectures in a low-query regime. Higher values indicate improved performance.

**Attack Success Rate.** In Figures 4 and 5, we show how many images reach at least 50% and 75% distance reduction over queries respectively. A sharper increase in this fraction signifies that more pairs experience substantial improvement more quickly. Again, once the turning point is reached between a pair, CGBA-H is implemented for further refinement.

**Success at a Fixed Low-Query Budget.** Figure 6 reports, at a low-query budget of 500 queries, the proportion of image pairs that reach or exceed various distance-reduction thresholds. TEA maintains a consistently higher proportion of successful pairs across nearly all thresholds, suggesting that its early-stage perturbations secure significant distance reductions more rapidly.

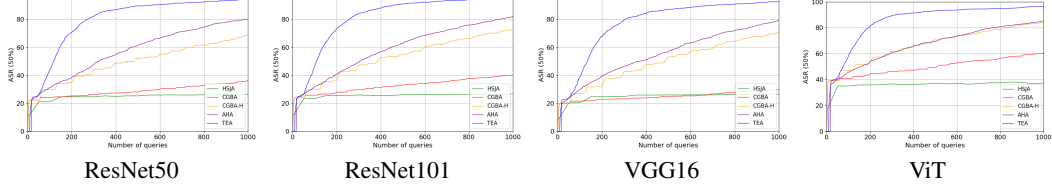


Figure 4: Comparison of ASR of 50% distance reduction. Higher values indicate that a higher proportion of images reach a distance reduction of 50% sooner.

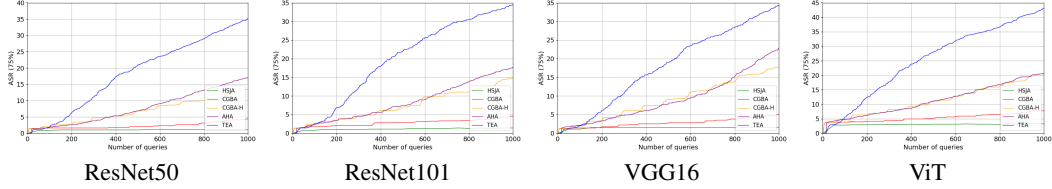


Figure 5: Comparison of ASR of 75% distance reduction. Higher values indicate that a higher proportion of images reach a distance reduction of 75% sooner.

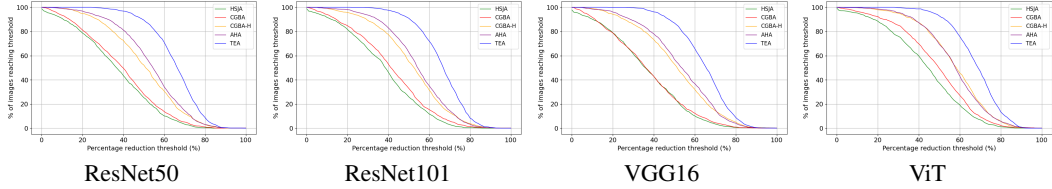


Figure 6: Cumulative distribution functions (CDFs) of distance reduction at 500 queries. Each curve represents the fraction of image pairs that achieve a given percentage reduction in the  $\ell_2$  distance, with higher values indicating a more effective reduction method.

**AUC Comparisons.** We assess the efficiency of our approach by computing the area under the median  $\ell_2$ -distance vs queries curve (AUC). Table 2 presents the AUC values for the low-query regime, up to the turning point. Across all architectures, TEA consistently yields lower AUC values.

Table 2: Average AUC values computed until the turning point across different architectures. Lower AUC values denote more effective early-stage distance reduction.

Model	HSJA	CGBA	CGBA-H	AHA	TEA
ResNet50	53575.41	52130.74	45745.09	44332.55	<b>35133.14</b>
ResNet101	52269.70	49487.56	43865.80	43542.48	<b>34189.94</b>
VGG16	53053.06	53226.27	45261.02	44756.50	<b>35790.23</b>
ViT	44377.75	41097.13	36788.92	37356.25	<b>30337.35</b>

**High-Query Performance with CGBA-H refinement.** Our hybrid TEA+CGBA-H strategy consistently matches or surpasses the state-of-the-art. Table 3 lists the median  $\ell_2$  distances upto 20000 queries. Note that CGBA-H is randomness-dependent. Further, it doesn’t re-explore when trapped in a narrow decision space and its stability can be unpredictable and subject to local decision boundary geometry. Figure 7 illustrates the median percentage reduction in the distance between the images.

## 5 Conclusion

In this work, we introduced *TEA*, a targeted, hard-label, black-box adversarial attack that leverages edge information from a target image to efficiently produce adversarial examples perceptually closer to a source image in low-query settings. *TEA* initially employs a global search that preserves prominent edge structures across the target image, subsequently refining the perturbations via patch-wise updates. Empirical results demonstrate that *TEA* significantly reduces the  $\ell_2$  distance between adversarial and source images, requiring over 70% fewer queries compared to current state-of-the-art



Table 3: Median  $\ell_2$  distances across different architectures. Here, TEA\* indicates using TEA until the turning point, and refining further with CGBA-H.

Query	ResNet50					Query	ResNet101				
	HSJA	CGBA	CGBA-H	AHA	TEA*		HSJA	CGBA	CGBA-H	AHA	TEA*
1000	86.800	80.709	58.815	52.069	<b>41.108</b>	1000	86.162	76.005	55.824	51.642	<b>40.090</b>
2500	85.262	69.031	39.701	33.165	<b>29.747</b>	2500	85.314	63.477	38.043	33.259	<b>29.965</b>
5000	83.345	48.703	22.835	18.394	<b>18.338</b>	5000	84.202	41.437	22.470	<b>18.780</b>	18.932
10000	81.623	22.094	10.214	<b>8.597</b>	8.798	10000	82.443	17.623	10.341	<b>9.021</b>	9.864
15000	80.642	10.999	5.908	6.757	<b>5.429</b>	15000	81.873	8.936	6.341	6.937	<b>6.281</b>
20000	79.605	6.594	4.185	6.449	<b>4.011</b>	20000	80.886	5.689	<b>4.507</b>	6.644	4.560

Query	VGG16					Query	ViT				
	HSJA	CGBA	CGBA-H	AHA	TEA*		HSJA	CGBA	CGBA-H	AHA	TEA*
1000	87.451	85.772	56.388	52.361	<b>41.578</b>	1000	79.212	64.516	49.394	49.541	<b>38.482</b>
2500	86.346	74.963	35.686	30.429	<b>27.984</b>	2500	78.739	44.789	32.573	34.762	<b>28.134</b>
5000	85.219	53.869	19.753	16.076	<b>16.050</b>	5000	78.170	25.118	18.566	22.197	<b>18.507</b>
10000	85.219	20.792	8.558	<b>7.456</b>	7.626	10000	77.786	10.319	<b>9.299</b>	11.267	9.416
15000	85.219	9.455	5.306	6.238	<b>4.979</b>	15000	77.087	<b>5.920</b>	5.987	8.180	6.301
20000	85.219	5.687	3.985	6.042	<b>3.823</b>	20000	76.727	<b>4.258</b>	4.635	7.404	4.955

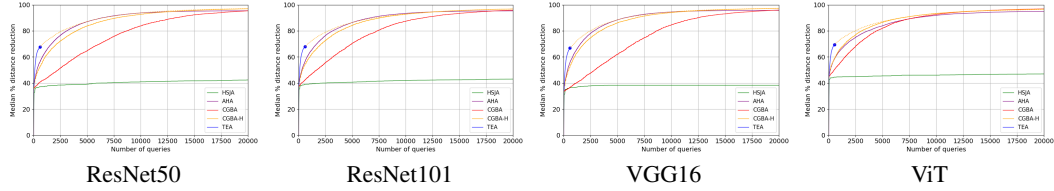


Figure 7: Comparison of median percentage decrease in  $\ell^2$  distance across different architectures, with higher values indicating a more effective reduction method.

methods. In addition, it also achieves reduced AUC and high ASR scores, indicating a consistently rapid reduction in distance to the source image across different models.

**Limitations.** (i) *Randomness*: Similar to state-of-the-art methods, TEA involves inherent randomness. In the patch-based refinement step, positions and sizes of patches are chosen randomly, leading to varying results across runs. Nevertheless, the overall performance remains stable when averaged over the thousand image pairs tested. (ii) *Low-query focus*: TEA is optimized specifically for scenarios with limited query budgets. Beyond this low-query regime, the method’s progress plateaus in a narrower decision space. However, the adversarial examples generated at this stage serve as strong initializations for subsequent refinement by other existing techniques.

**Future Work.** Several extensions could enhance TEA: (a) substituting edge information with other features such as textures, color distributions, or high-frequency components; (b) training a surrogate model based on query data already collected to guide subsequent perturbations and (c) developing defense mechanisms capable of mitigating attacks based on structure-preserving perturbations.

## Code Availability

Our code is available at the following URL: <https://github.com/mdppml/TEA>.

## Code of Ethics and Broader Impact Statement

We evaluate TEA exclusively on the publicly available ImageNet-1K validation set, which is distributed for non-commercial research and educational use under the ImageNet access agreement. The dataset contains no personally identifiable information, and we used it in accordance with the applicable license terms. As TEA reduces the number of required queries for targeted hard-label attacks in a low-query setting, it could be leveraged to more rapidly craft adversarial inputs against commercial or safety-critical vision systems. We encourage practitioners to adopt defense mechanisms that go

beyond detecting frequency-based perturbations, explicitly incorporating checks for edge-informed distortions, and defenses attuned to other structural features, to guard against similar attacks.

## Acknowledgements

This research was supported by the German Federal Ministry of Education and Research (BMBF) under project number 01ZZ2010 and partially funded through grant 01ZZ2316D (PrivateAIM). The authors acknowledge the usage of the Training Center for Machine Learning (TCML) cluster at the University of Tübingen.

## References

- [1] Robert Bassett, Mitchell Graves, and Patrick Reilly. Color and edge-aware adversarial image perturbations. *arXiv preprint arXiv:2008.12454*, 2020.
- [2] Mariusz Bojarski, Davide Del Testa, Daniel Dworakowski, Bernhard Firner, Beat Flepp, Praseem Goyal, Lawrence D Jackel, Mathew Monfort, Urs Muller, Jiakai Zhang, et al. End to end learning for self-driving cars. *arXiv preprint arXiv:1604.07316*, 2016.
- [3] Wieland Brendel, Jonas Rauber, and Matthias Bethge. Decision-based adversarial attacks: Reliable attacks against black-box machine learning models. *arXiv preprint arXiv:1712.04248*, 2017.
- [4] Thomas Brunner, Frederik Diehl, Michael Truong Le, and Alois Knoll. Guessing smart: Biased sampling for efficient black-box adversarial attacks. In *Proceedings of the IEEE/CVF International Conference on Computer Vision*, pages 4958–4966, 2019.
- [5] Chenyi Chen, Ari Seff, Alain Kornhauser, and Jianxiong Xiao. Deepdriving: Learning affordance for direct perception in autonomous driving. In *Proceedings of the IEEE international conference on computer vision*, pages 2722–2730, 2015.
- [6] Jianbo Chen, Michael I Jordan, and Martin J Wainwright. Hopskipjumpattack: A query-efficient decision-based attack. In *2020 IEEE Symposium on Security and Privacy (SP)*, pages 1277–1294. IEEE, 2020.
- [7] Jia Deng, Wei Dong, Richard Socher, Li-Jia Li, Kai Li, and Li Fei-Fei. Imagenet: A large-scale hierarchical image database. In *2009 IEEE conference on computer vision and pattern recognition*, pages 248–255. Ieee, 2009.
- [8] Alexey Dosovitskiy, Lucas Beyer, Alexander Kolesnikov, Dirk Weissenborn, Xiaohua Zhai, Thomas Unterthiner, Mostafa Dehghani, Matthias Minderer, Georg Heigold, Sylvain Gelly, et al. An image is worth 16x16 words: Transformers for image recognition at scale. *arXiv preprint arXiv:2010.11929*, 2020.
- [9] Andre Esteva, Brett Kuprel, Roberto A Novoa, Justin Ko, Susan M Swetter, Helen M Blau, and Sebastian Thrun. Dermatologist-level classification of skin cancer with deep neural networks. *nature*, 542(7639): 115–118, 2017.
- [10] Robert Geirhos, Patricia Rubisch, Claudio Michaelis, Matthias Bethge, Felix A Wichmann, and Wieland Brendel. Imagenet-trained cnns are biased towards texture; increasing shape bias improves accuracy and robustness. In *International conference on learning representations*, 2018.
- [11] Ian J Goodfellow, Jonathon Shlens, and Christian Szegedy. Explaining and harnessing adversarial examples. *arXiv preprint arXiv:1412.6572*, 2014.
- [12] Kaiming He, Xiangyu Zhang, Shaoqing Ren, and Jian Sun. Deep residual learning for image recognition. In *Proceedings of the IEEE conference on computer vision and pattern recognition*, pages 770–778, 2016.
- [13] Andrew Ilyas, Logan Engstrom, Anish Athalye, and Jessy Lin. Black-box adversarial attacks with limited queries and information. In *International conference on machine learning*, pages 2137–2146. PMLR, 2018.
- [14] Huichen Li, Xiaojun Xu, Xiaolu Zhang, Shuang Yang, and Bo Li. Qeba: Query-efficient boundary-based blackbox attack. In *Proceedings of the IEEE/CVF conference on computer vision and pattern recognition*, pages 1221–1230, 2020.

- [15] Jie Li, Rongrong Ji, Peixian Chen, Baochang Zhang, Xiaopeng Hong, Ruixin Zhang, Shaoxin Li, Jilin Li, Feiyue Huang, Shaoqing Ren, and Yongjian Sun, JiWu. Aha! adaptive history-driven attack for decision-based black-box models. In *Proceedings of the IEEE/CVF International Conference on Computer Vision*, pages 16168–16177, 2021.
- [16] Yujia Liu, Seyed-Mohsen Moosavi-Dezfooli, and Pascal Frossard. A geometry-inspired decision-based attack. In *Proceedings of the IEEE/CVF International Conference on Computer Vision*, pages 4890–4898, 2019.
- [17] Chen Ma, Xiangyu Guo, Li Chen, Jun-Hai Yong, and Yisen Wang. Finding optimal tangent points for reducing distortions of hard-label attacks. *Advances in Neural Information Processing Systems*, 34: 19288–19300, 2021.
- [18] Thibault Maho, Teddy Furon, and Erwan Le Merrer. Surf-free: a fast surrogate-free black-box attack. In *Proceedings of the IEEE/CVF conference on computer vision and pattern recognition*, pages 770–778, 2016.
- [19] Md Farhamdur Reza, Ali Rahmati, Tianfu Wu, and Huaiyu Dai. Cgba: Curvature-aware geometric black-box attack. In *Proceedings of the IEEE/CVF international conference on computer vision*, pages 124–133, 2023.
- [20] Karen Simonyan and Andrew Zisserman. Very deep convolutional networks for large-scale image recognition. *arXiv preprint arXiv:1409.1556*, 2014.
- [21] Irvin Sobel. Neighborhood coding of binary images for fast contour following and general binary array processing. *Computer graphics and image processing*, 8(1):127–135, 1978.
- [22] Fnu Suya, Jianfeng Chi, David Evans, and Yuan Tian. Hybrid batch attacks: Finding black-box adversarial examples with limited queries. In *29th USENIX security symposium (USENIX Security 20)*, pages 1327–1344, 2020.
- [23] Christian Szegedy, Wojciech Zaremba, Ilya Sutskever, Joan Bruna, Dumitru Erhan, Ian Goodfellow, and Rob Fergus. Intriguing properties of neural networks. *arXiv preprint arXiv:1312.6199*, 2013.
- [24] Yusuke Tashiro, Yang Song, and Stefano Ermon. Diversity can be transferred: Output diversification for white-and black-box attacks. *Advances in neural information processing systems*, 33:4536–4548, 2020.
- [25] Xiaosen Wang, Zeliang Zhang, Kangheng Tong, Dihong Gong, Kun He, Zhifeng Li, and Wei Liu. Triangle attack: A query-efficient decision-based adversarial attack. In *European conference on computer vision*, pages 156–174. Springer, 2022.
- [26] Matthew D Zeiler and Rob Fergus. Visualizing and understanding convolutional networks. In *Computer Vision–ECCV 2014: 13th European Conference, Zurich, Switzerland, September 6–12, 2014, Proceedings, Part I 13*, pages 818–833. Springer, 2014.